MIMO-NOMA Networks Relying on Reconfigurable Intelligent Surface: A Signal Cancellation Based Design

Tianwei Hou, *Student Member, IEEE,* Yuanwei Liu, *Senior Member, IEEE,*

Zhengyu Song, Xin Sun, and Yue Chen, *Senior Member, IEEE,*

Abstract

Reconfigurable intelligent surface (RIS) technique stands as a promising signal enhancement or signal cancellation technique for next generation networks. We design a novel passive beamforming weight at RISs in a multiple-input multiple-output (MIMO) non-orthogonal multiple access (NOMA) network for simultaneously serving paired users, where a signal cancellation based (SCB) design is employed. In order to implement the proposed SCB design, we first evaluate the minimal required number of RISs in both the diffuse scattering and anomalous reflector scenarios. Then, new channel statistics are derived for characterizing the effective channel gains. In order to evaluate the network's performance, we derive the closed-form expressions both for the outage probability (OP) and for the ergodic rate (ER). The diversity orders as well as the high-signal-to-noise (SNR) slopes are derived for engineering insights. The network's performance of a finite resolution design has been evaluated. Our analytical results demonstrate that: i) the inter-cluster interference can be eliminated with the aid of large number of RIS elements; ii) the line-of-sight of the BS-RIS and RIS-user links are required for the diffuse scattering scenario, whereas the LoS links are not compulsory for the anomalous reflector scenario.

Index Terms

T. Hou, Z. Song and X. Sun are with the School of Electronic and Information Engineering, Beijing Jiaotong University, Beijing 100044, China (email: 16111019@bjtu.edu.cn, songzy@bjtu.edu.cn, xsun@bjtu.edu.cn).

Y. Liu and Yue Chen are with School of Electronic Engineering and Computer Science, Queen Mary University of London, London E1 4NS, U.K. (e-mail: yuanwei.liu@qmul.ac.uk, yue.chen@qmul.ac.uk).

MIMO, NOMA, passive beamforming, reconfigurable intelligent surface, signal cancellation.

I. Introduction

The demanding for having high spectrum efficiency (SE) and energy efficiency (EE) has been rapidly increasing in next-generation (NG) networks [2]. A promising access technique, non-orthogonal multiple access (NOMA), has been proposed, which is capable of simultaneously serving multiple users at different quality-of-service requirements [3]–[5]. Multiple users share the same time/frequency/code resource block by with the aid of superposition coding (SC) at the transmitter and successive interference cancellation (SIC) at the receiver by capitalizing the difference of users' channel state information (CSI) [6]–[8].

Since multiple antennas (MAs) offer extra diversity by its spacial domain, MA techniques are of significant importance. The application of MA techniques assisted NOMA networks has attached significant attention. In classic multiple-input multiple-output (MIMO) designs, the base (BS) equipped with M transmitting antennas (TAs) is capable of transmitting maximal M interference-free beams. However, since multiple users are paired to perform NOMA in each cluster, the BS equipped with M TAs has to compulsorily serve KM users simultaneously, where K denotes the number of users in each cluster. Hence, how to design interference-free beamforming becomes an interesting problem, which is valuable to examine. A zero-forcing-based (ZF-based) design was proposed in [9], where the active beamforming at the BS is an identity matrix. However, there are two drawbacks, where 1) the number of receiving antennas (RAs) has to be higher than that of the BS to ensure the existence of a solution; and 2) due to the property of singular value decomposition, the antenna gain of the ZF-based design can be obtained as $L - M + 1$, where L denotes the number of RAs. Then a signal-alignment-based (SA-based) design is proposed to release the constraint of the number of RAs [10], which relies on the gain shifting of user's channel matrixes. By doing so, the small-scale channel gains of K users in each cluster are identical, but correspond to different distances, and hence MK users can be treated as M users. It is demonstrated that multi-user NOMA networks may be not practical due to high computational complexity [11]. Numerous applications related to MIMO-NOMA were proposed, i.e. MIMO-NOMA enhanced physical layer security networks [12] and MIMO-NOMA enhanced simultaneous wireless information and power transfer (SWIPT) networks [13].

However, as mentioned above, there were many constrains on the number of RAs in the previous designs.

Recently, reconfigurable intelligent surface (RIS) technique stands as the next generation relay technique, also namely relay 2.0, received considerable attention due to its high EE [14]–[17]. The RIS elements are capable of independently shifting the signal phase and absorbing the signal energy, and hence the reflected signals can be boosted or diminished for wireless transmission [18]–[20]. By doing so, numerous application scenarios have been considered, e.g. RIS-aided coverage enhancement. The RIS elements are normally deployed on the building or on the wall [21]. A novel three-dimension design for aerial RIS network was proposed in [22], where RIS elements are employed at aerial platforms, and hence a full-angle reflection can be implemented. Currently, RIS networks are simply separated into two categories [23], i.e. anomalous reflector or diffuse scatterer for mmWave and sub-6G networks, respectively. The coverage distance is reduced in mmWave networks [24], and hence more users are located in coverage-holes compared to conventional networks. Thus, reflected signals can be aligned by RISs for serving users located in the coverage-holes [25].

NOMA and RIS techniques can be naturally integrated for enhancing both SE and EE. The RISs can be deployed for the cell-edge users in the NOMA networks, where the reflected signal cannot be received at the cell-center users [26]. An one-bit coding scheme was invoked in the RIS-aided NOMA networks, where imperfect SIC scenario was evaluated in [27]. Since both the BS and RISs are pre-deployed, and hence the line-of-sight (LoS) links between the BS and RISs are expected for improving desired signal power [28]. The Rician fading channels were utilized for illustrating the channel gain of both the BS-RIS and RIS-user links in [29]. A SISO-NOMA network was proposed in [30], where a prioritized design was proposed for further enhancing the network's SE and EE. However, previous contributions mainly focus on the signal enhancement based (SEB) designs, where signals are boosted at the user side or at the BS side.

A. Motivations and Contributions

Previous contributions mainly focus on the SEB designs, whilst there is a paucity of investigations on the signal-cancellation-based (SCB) design of the RIS-aided networks. Inspired by the concepts of the signal cancellation [31], [32], we propose a novel SCB design concept, which provides the desired degree of flexibility for the RIS-aided networks. In the MIMO-NOMA

networks, one of key challenge is to eliminate the inter-cluster interference. Hence, in order to illustrate the potential benefits provided by RISs, a RIS-aided SCB design in MIMO-NOMA networks is proposed for comprehensively analyzing the performance of the networks.

Against to above background, our contributions can be summarized as follows:

- We propose a novel SCB design in RIS-aided MIMO-NOMA networks, where the inter-cluster interference can be eliminated for enhancing the network's performance. The impacts of both the diffuse scattering and anomalous reflector scenarios are exploited. The impact of the proposed design on the attainable performance is characterized.

- We first derive the minimal required number of RISs for implementing the proposed SCB design. For the ideal-RIS (I-RIS) cases, our analytical results illustrate that the inter-cluster interference can be beneficially eliminated. We then evaluate the impact of non-ideal-RIS (NI-RIS) cases by finite resolution techniques.

- Explicitly, we derive closed-form expressions of both the OP and of the ER for the proposed SCB design. The exact closed-form expressions of the OP and of the ER are derived in both the diffuse scattering and anomalous reflector scenarios. The diversity orders and high-SNR slopes are derived based on the OP and ER. The results confirm that the diversity order is obtained as the number of RAs.

- Our analytical results illustrate that the proposed SCB design is capable of 1) releasing the constraint of the number of RAs; 2) perfectly eliminating the inter-cluster interference in the I-RIS cases. The simulation results confirm our analysis, illustrating that: 1) the outage floors and ergodic ceilings occur for the NI-RIS cases; 2) the proposed SCB design does not rely on a high number of RISs for increasing both the OP and ER. 3) the proposed SCB design is capable of outperforming the classic ZF-based and SA-based designs.

B. Organization and Notations

In Section II, a SCB design is investigated in RIS-aided MIMO-NOMA networks. The minimal required number of RISs is analyzed. Then the passive beamforming weight at RISs is proposed for implementing SCB design. Analytical results are presented in Section III to show the performance of the proposed SCB design. In Section IV, the numerical results are provided for verifying our analysis. Then Section V concludes this article. $\mathbb{P}(\cdot)$ denotes the probability, and $\mathbb{E}(\cdot)$ denotes the expectation. $\mathbf{H}^T$, $\mathbf{H}^H$, $rank(\mathbf{H})$ denote the transpose and conjugate transpose,

TABLE I:
TABLE OF NOTATIONS

$R_{m,k}$	The target rate of user k in cluster m.
$\mathcal{K}_1$	Fading factor between the BS and RISs.
$\mathcal{K}_2$	Fading factor between the RISs and users.
M	The number of TAs.
L	The number of RAs.
K	The number of users in each cluster.
N	The number of RISs.
$\mathbf{H}$	The channel matrix of the BS-RIS link.
$\mathbf{G}_{m,k}$	The channel matrix between the RISs and user k in cluster m.
$\mathbf{W}_{m,k}$	The channel matrix between the BSs and user k in cluster m.
$\mathbf{\Phi}$	The effective matrix of RISs.

as well as rank of the matrix $\mathbf{H}$. $\|\bullet\|_2^2$ denotes the Frobenius norm. Table I lists some critical notations used in this article.

II. SYSTEM MODEL

Let us focus our attention on a MIMO-NOMA network in downlink communication, where a BS equipped with M TAs is simultaneously communicating with MK users each equipped with L RAs by utilizing the power-domain NOMA techniques. For simplicity, MK users are separated into M clusters, and K users are paired in each cluster. We have N intelligent surfaces at a proper location with $N \geq 1$ for implementing wireless communication. By properly controlling the amplitude coefficients and phase shifts of each RIS element, the signals can be beneficially manipulated. The system model is illustrated in Fig. 1.

A. System Description of RIS-aided MIMO-NOMA Networks

Since the LoS link does not exist in the BS-user link, the small-scale fading matrix between the BS and user k in cluster m is defined by Rayleigh fading channels, which can be expressed as

$$\mathbf{W}_{m,k} = \begin{bmatrix} w_{1,1}^{m,k} & \cdots & w_{1,M}^{m,k} \\ \vdots & \cdots & \vdots \\ w_{L,1}^{m,k} & \cdots & w_{1,1}^{m,k} \end{bmatrix}, \tag{1}$$
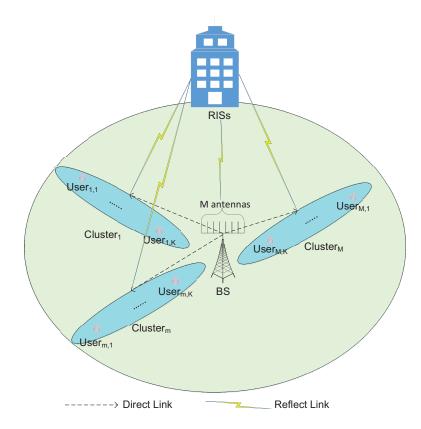
Fig. 1: System model of the RIS-aided MIMO-NOMA networks.

where $\mathbf{W}_{m,k}$ is a $(L \times M)$ element matrix. Note that the probability density function (PDF) of the Rayleigh fading channel gains is given by

$$f(x) = e^{-x}. \tag{2}$$

The large-scale fading between the BS and user k in cluster m is given by

$$L_{\mathrm{b},m,k} = d_{\mathrm{b},m,k}^{-\alpha_3}, \tag{3}$$

where α_3 denotes the path loss exponent between the BS and user k in cluster m.

Since the LoS links are expected for both the BS-RIS and RIS-user links, the channel matrixes

are defined by Rician fading channels as follows:

$$
\mathbf{H} = \begin{bmatrix} h_{1,1} & \cdots & h_{1,M} \\ \vdots & \cdots & \vdots \\ h_{N,1} & \cdots & h_{N,M} \end{bmatrix},
\tag{4}
$$

where $\mathbf{H}$ is a $(N \times M)$ Rician fading channel gains, which can be modeled as follows:

$$
h_{n,m} = \sqrt{\frac{\mathcal{K}_1}{\mathcal{K}_1 + 1}} h_{n,m}^{\mathrm{LoS}} + \sqrt{\frac{1}{\mathcal{K}_1 + 1}} h_{n,m}^{\mathrm{NLoS}},
\tag{5}
$$

where $\mathcal{K}_1$ denotes the Rician factor of the BS-RIS link. $h_{n,m}^{\mathrm{LoS}}$ and $h_{n,m}^{\mathrm{NLoS}}$ denote the LoS and Non-LoS (NLoS) components, respectively.

Similar to (4), the small-scale fading matrix between the RISs and user k in cluster m is defined as

$$
\mathbf{G}_{m,k} = \begin{bmatrix} g_{1,1}^{m,k} & \cdots & g_{1,N}^{m,k} \\ \vdots & \cdots & \vdots \\ g_{L,1}^{m,k} & \cdots & g_{L,N}^{m,k} \end{bmatrix},
\tag{6}
$$

where $\mathbf{G}_{m,k}$ is $(L \times N)$ matrix whose elements represent Rician fading channel gains with fading parameter $\mathcal{K}_2$. Similarly, the channel gains of the RIS-user link is given by

$$
g_{l,n}^{m,k} = \sqrt{\frac{\mathcal{K}_2}{\mathcal{K}_2 + 1}} g_{l,n}^{m,k,\mathrm{LoS}} + \sqrt{\frac{1}{\mathcal{K}_2 + 1}} g_{l,n}^{m,k,\mathrm{NLoS}},
\tag{7}
$$

where $\mathcal{K}_2$ denotes the Rician factor of the BS-RIS link. $g_{l,n}^{m,k,\mathrm{LoS}}$ and $g_{l,n}^{m,k,\mathrm{NLoS}}$ denote the LoS and NLoS components, respectively.

In this article, d_1 and $d_{m,k}$ represent the distances of the BS-RIS and RIS-user links. In order to limit the inter-cluster interference, the received signal power levels of both the BS-user and reflected links are expected to the same order. Recently, anomalous reflecting and diffuse scattering scenarios are presented for the mmWave and sub-6G networks, respectively [33]. On the one hand, the size of RISs is comparable with the wavelength for the sub-6G networks, and hence the RISs are expected to be diffusers. Such as radar networks, the path loss of reflected links are expected as product-distance law [34]. On the other hand, the wavelength is sufficiently small compared with the size of RISs, hence the theory of geometric optics is

capable of modeling the path loss, where the sum-distance law of a specular reflection holds in the anomalous reflector scenarios based on the generalized Snell's law. We then study the feasibility of two scenarios, where the RISs act as anomalous reflectors or diffuse scatterers.

1) *Diffuse Scattering Scenario:* When the size of RISs is comparable with the wavelength, where the size of RIS elements is usually set to $\frac{1}{4}$ wavelength, the RISs are considered as diffuse scatters [33]. Therefore, the large-scale fading between the BS and user k through RISs can be expressed as

$$L_{\mathrm{D},m,k} = d_1^{-\alpha_1} d_{m,k}^{-\alpha_2}, \tag{8}$$

where α_1 and α_2 denote the path loss exponent of the BS-RIS and RIS-user links, respectively. We then discuss the minimal required number of RISs for the diffuse scattering scenario in the following Lemma.

Lemma 1. *Assuming that the small-scale fading environments of BS-RIS, RIS-user and BS-user links are strong enough, i.e. $\mathcal{K}_1 = \mathcal{K}_2 \sim \infty$, where the elements in fading matrixes are all one. Hence, the following constraint in diffuse scattering scenario needs to be met for implementing the proposed SCB design:*

$$N^2 \geq \frac{(M-1)^2 d_{\mathrm{b},m,k}^{-\alpha_3}}{d_1^{-\alpha_1} d_{m,k}^{-\alpha_2}}. \tag{9}$$

Proof: In order to limit the inter-cluster interference, the power level of the reflected signals need to be higher than that of the BS-user links. Thus, the following constraint needs to be met [35]:

$$N d_1^{-\frac{\alpha_1}{2}} d_{m,k}^{-\frac{\alpha_2}{2}} \geq (M-1) d_{\mathrm{b},m,k}^{-\frac{\alpha_3}{2}}. \tag{10}$$

After some algebraic manipulations, the results in (9) *can be readily obtained. Thus, the proof is complete.* ∎

2) *Anomalous Reflector Scenario:* We the turn our attention to the anomalous reflector scenario, where the frequency of wave is usually sufficiently high, the large-scale fading can be considered as anomalous reflectors [33]. Therefore, the large-scale fading between the BS and user k through RISs can be expressed as

$$L_{\mathrm{A},m,k} = (d_1 + d_{m,k}^{\frac{\alpha_2}{\alpha_1}})^{-\alpha_1}. \tag{11}$$

TABLE II:
FEASIBILITY ANALYSIS

RIS Mode	α_1	α_2	α_3	N
	3.5	3.5	3.5	1449
Diffuse scattering	2.2	3.5	3.5	84
	2.2	2.2	3.5	5
	3.5	3.5	3.5	3
Anomalous reflector	2.2	3.5	3.5	1
	2.2	2.2	3.5	1

If $\alpha_1 = \alpha_2$, the large-scale fading can be simplified to

$$L_{\mathrm{A},m,k} = (d_1 + d_{m,k})^{-\alpha_1}. \tag{12}$$

Lemma 2. *Let us assume that the small-scale fading environments of BS-RIS, RIS-user and BS-user links are strong enough, i.e. $\mathcal{K}_1 = \mathcal{K}_2 \sim \infty$, where the elements in fading matrixes are all one. Hence, the following constraint in anomalous reflector scenario needs to be met for implementing the proposed SCB design:*

$$N^2 \geq \frac{(M-1)^2 d_{\mathrm{b},m,k}^{-\alpha_3}}{(d_1 + d_{m,k}^{\frac{\alpha_2}{\alpha_1}})^{-\alpha_1}}. \tag{13}$$

Proof: Similar to **Lemma 1***, and by utilizing* (11)*, the results in* (13) *can be obtained.* ∎

Then we conclude the feasibility of two alternatives scenarios in Table II, and we set $d_1 = d_{m,k} = 80$m and $d_{\mathrm{b},m,k} = 100$m. N represents the minimal required number of RISs.

Remark 1. *The results in* TABLE II *demonstrate that the proposed SCB design is only applicable for the case of $\alpha_1 > \alpha_3$ and $\alpha_2 > \alpha_3$ in the diffuse scattering scenario.*

Remark 2. *The results in* TABLE II *demonstrate that the proposed SCB design can be beneficially implemented in the anomalous reflector scenarios for the case that both the BS-RIS and RIS-user links experience Rayleigh fading channels.*

B. Passive Beamforming Designs

We first pay our attention to the signal model, and the information bearing vector at the BS can be expressed as:

$$\mathbf{s} = \begin{bmatrix} \alpha_1 s_{1,1} + \cdots + \alpha_K s_{1,K} \\ \vdots \\ \alpha_1 s_{M,1} + \cdots + \alpha_K s_{M,K} \end{bmatrix}, \tag{14}$$

where $s_{m,k}$ denotes the signal intended for user k in cluster m. α_k represents the power allocation factor for user k. Based on the NOMA protocol, we have $\sum_{k=1}^{K} \alpha_k^2 = 1$.

Without loss of generality, we focus on user k in cluster m. Thus, the receiving signal at user k in cluster m is given by

$$y_{m,k} = \left(\mathbf{G}_{m,k} \mathbf{\Phi} \mathbf{H} \sqrt{L_{m,k}} + \mathbf{W}_{m,k} \sqrt{L_{b,m,k}} \right) \mathbf{P} p \mathbf{s} + N_0, \tag{15}$$

where p denotes the transmit power at the BS, $\mathbf{P}$ denotes the precoding matrix, $\mathbf{\Phi} \triangleq \mathrm{diag} \left[\beta_1 \phi_1, \beta_2 \phi_2, \cdots, \beta_N \phi_N \right]$ denotes both the effective phase shifts and amplitude coefficients by RISs. More specifically, $\beta_n \in (0, 1]$ denotes the amplitude coefficient of RIS element n, $\phi_n = \exp(j\theta_n), j = \sqrt{-1}, \forall n = 1, 2 \cdots, N$. $\theta_n \in [0, 2\pi)$ denotes the phase shift by RIS element n. Finally, the additive white Gaussian noise (AWGN) is denoted by N_0, which is a zero-mean complex circularly symmetric Gaussian variable with variance σ^2. In order to implement the proposed SCB design, the CSIs are assumed to perfectly known at the RIS controller [36].

In practice, user k in cluster m applies a detection vector $\mathbf{v}_{k,m}$ to its received signals, therefore the users observations is given by:

$$\tilde{y}_{m,k} = \mathbf{v}_{k,m}^H \left(\mathbf{G}_{m,k} \mathbf{\Phi} \mathbf{H} \sqrt{L_{m,k}} + \mathbf{W}_{m,k} \sqrt{L_{b,m,k}} \right) \mathbf{P} p \mathbf{s} + \mathbf{v}_{k,m}^H N_0. \tag{16}$$

In order to provide a general framework, we assume that the active beamformer weights at the BS obey:

$$\mathbf{P} = \mathbf{I}_M, \tag{17}$$

where $\mathbf{I}_M$ represents a $M \times M$ identity matrix. The detection vectors of users can be expressed as all one vector as:

$$\mathbf{v}_{k,m}^H = \begin{bmatrix} 1 & \cdots & 1 \end{bmatrix}. \tag{18}$$

We then turn our attention to the passive beamforming design at the RISs, where the phase shifts and reflection amplitude coefficients are jointly manipulated. In this article, the passive beamforming design at RISs mainly focuses on interference cancellation, and hence we first remove the m-th column of the matrix $\mathbf{W}_{m,k}$ as follows:

$$\bar{\mathbf{W}}_{m,k} = \left[\begin{array}{ccccccc} \mathbf{w}_1 & \cdots & \mathbf{w}_{m-1} & \mathbf{w}_{m+1} & \cdots & \mathbf{w}_M \end{array} \right], \tag{19}$$

where $\mathbf{w}_{m-1}$ denotes the $(m-1)$-th column of the matrix $\mathbf{W}_{m,k}$. Since the elements in the active beamforming weight and detection vectors are all one, the effective inter-cluster interference of all MK users can be expressed as follows:

$$\mathbf{B} = \left[\begin{array}{c} -\bar{\mathbf{W}}_{1,1}\mathbf{1}_{M-1}\sqrt{L_{\mathrm{b},1,1}} \\ \vdots \\ -\bar{\mathbf{W}}_{1,K}\mathbf{1}_{M-1}\sqrt{L_{\mathrm{b},1,K}} \\ \vdots \\ -\bar{\mathbf{W}}_{M,K}\mathbf{1}_{M-1}\sqrt{L_{\mathrm{b},M,K}} \end{array} \right], \tag{20}$$

where $\mathbf{1}_{M-1} = [1, 1, \cdots, 1]^{\mathrm{T}}$ denotes an $((M-1) \times 1)$ all one vector.

In order to design the passive beamforming weight at RISs, we first define an effective matrix in the diffuse scattering scenarios by stacking the channel gains of all MK users as follows:

$$\tilde{\mathbf{H}}_{\mathrm{D}} = \left[\begin{array}{ccc} g_{1,1}^{1,1}h_{1,1}\sqrt{L_{\mathrm{D},1,1}} & \cdots & g_{1,N}^{1,1}h_{N,1}\sqrt{L_{\mathrm{D},1,1}} \\ \vdots & \cdots & \vdots \\ g_{L,1}^{1,1}h_{1,M}\sqrt{L_{\mathrm{D},1,1}} & \cdots & g_{L,N}^{1,1}h_{N,M}\sqrt{L_{\mathrm{D},1,1}} \\ \vdots & \cdots & \vdots \\ g_{L,1}^{M,K}h_{1,M}\sqrt{L_{\mathrm{D},M,K}} & \cdots & g_{L,N}^{M,K}h_{N,M}\sqrt{L_{\mathrm{D},M,K}} \end{array} \right], \tag{21}$$

where $\tilde{\mathbf{H}}_{\mathrm{D}}$ is a $(LKM) \times N$ element matrix. Then we define an effective RIS vector $\widetilde{\boldsymbol{\Phi}} = [\beta_1\phi_1, \beta_2\phi_2, \cdots, \beta_N\phi_N]^{\mathrm{T}}$, which is an $N \times 1$ effective vector. Hence, in order to limit the inter-cluster interference at each user in the diffuse scattering scenarios, the following constraint needs to be met:

$$\tilde{\mathbf{H}}_{\mathrm{D}}\widetilde{\boldsymbol{\Phi}} = \mathbf{B}. \tag{22}$$

To achieve the ambitions design objective, the solution of RISs can be given as follows:

$$\widetilde{\mathbf{\Phi}} = \tilde{\mathbf{H}}_{\mathrm{D}}^{-1}\mathbf{B}. \tag{23}$$

Similarly, let us define an effective matrix for the anomalous reflector scenarios as follows:

$$\tilde{\mathbf{H}}_{\mathrm{A}} = \begin{bmatrix} g_{1,1}^{1,1}h_{1,1}\sqrt{L_{\mathrm{A},1,1}} & \cdots & g_{1,N}^{1,1}h_{N,1}\sqrt{L_{\mathrm{A},1,1}} \\ \vdots & \cdots & \vdots \\ g_{L,1}^{1,1}h_{1,M}\sqrt{L_{\mathrm{A},1,1}} & \cdots & g_{L,N}^{1,1}h_{N,M}\sqrt{L_{\mathrm{A},1,1}} \\ \vdots & \cdots & \vdots \\ g_{L,1}^{M,K}h_{1,M}\sqrt{L_{\mathrm{A},M,K}} & \cdots & g_{L,N}^{M,K}h_{N,M}\sqrt{L_{\mathrm{A},M,K}} \end{bmatrix}. \tag{24}$$

Then, the RISs can be designed as follows:

$$\widetilde{\mathbf{\Phi}} = \tilde{\mathbf{H}}_{\mathrm{A}}^{-1}\mathbf{B}. \tag{25}$$

Note that we have $rank(\tilde{\mathbf{H}}_{\mathrm{A}}) = rank(\tilde{\mathbf{H}}_{\mathrm{D}}) \leq MKL$, thus for the case of $N < MKL$, there exists no solution for passive beamforming at RISs, which satisfy the constraints of $\theta_n \in [0, 2\pi)$ and $\beta_n \in (0, 1]$, $\forall n = 1 \cdots N$.

Remark 3. *In order to obtain the solution in* (23) *and in* (25)*, the constraint of the number of RISs* $N > MKL$ *needs to be met, otherwise no solution satisfying* $\beta_n \in (0, 1]$ *can be obtained.*

Lemma 3. *Based on* **Lemma 1** *and* **Lemma 2** *as well as* **Remark 3***, the following constraints for both the diffuse scattering and anomalous reflector scenarios need to be met for the proposed SCB design:*

$$N_{\mathrm{D}} \geq \max\left\{(M-1)L_{\mathrm{D}}, MKL\right\}, \tag{26}$$

and

$$N_{\mathrm{S}} \geq \max\left\{(M-1)L_{\mathrm{S}}, MKL\right\}, \tag{27}$$

where $L_{\mathrm{D}} = \left(\dfrac{d_{\mathrm{b},m,k}^{-\alpha_3}}{d_1^{-\alpha_1}d_{m,k}^{-\alpha_2}}\right)^{\frac{1}{2}}$ *and* $L_{\mathrm{S}} = \left(\dfrac{d_{\mathrm{b},m,k}^{-\alpha_3}}{(d_1+d_{m,k}^{\alpha_1})^{\frac{\alpha_2}{\alpha_1}}}\right)^{\frac{1}{2}}$.

Remark 4. *Since the signals cannot be amplified by RISs, the minimal number of RISs is required*

to be greater than (26) *and* (27) *for the diffuse scattering and anomalous reflector scenarios, respectively.*

In this article, K users are paired to perform NOMA in each cluster, and thus based on the proposed passive beamforming design at RISs, the signal-to-interference-plus-noise ratio (SINR) of user k in cluster m for the I-RIS cases in both the diffuse scattering and anomalous reflector scenarios can be expressed as

$$SINR_{k,m} = \frac{\left| w^{m,k} \right|^2 L_{b,m,k} p \alpha_k^2}{\sum\limits_{n=k+1}^{K} \left| w^{m,k} \right|^2 L_{b,m,k} p \alpha_n^2 + L\sigma^2}, \tag{28}$$

where $\left| w^{m,k} \right|^2$ denotes the effective channel gain of user k in cluster m, which will be evaluated in the next section.

C. RIS Designs for Finite Resolutions

In most previous research, perfect RIS assumption was assumed, and hence the amplitude coefficients and phase shifts are continuous. However, in practice, the amplitude coefficients and phase shifts rely on the diodes employed at RISs [36]. Thus the discrete phase shifts were considered [37]. Both perfect and imperfect phase shifters were considered in [38], [39]. In this article, the amplitude coefficients β and phase shifts θ may be not continuous due to the hardware limitations. We then consider an alternative low-cost implementation for applying multi-bit control to RISs, i.e. each diagonal element of Φ is selected from a set of discrete finite resolutions. It is also worth mentioning that several amplitude dividers may be employed at the RIS elements, whereas the current hardware design of RISs only contains several phase shifters. As such, the RIS performs a linear mapping based on an equivalent amplitude-coefficient vector as well as phase-shift vector. It is assumed that the phase shifts and amplitude coefficients at RISs take a finite number of discrete values. The number of bits b is used to indicate the number of phase shift and amplitude coefficient levels T with $T = 2^b$, and hence the discrete phase shift and amplitude coefficient values can be uniformly mapped to the interval $[0, 2\pi)$ and $[0, 1]$, respectively. Thus, the set of discrete amplitude coefficient as well as phase values at each RIS element can be given by

$$\widehat{\theta} = \{0, \Delta\theta, \cdots (T-1)\Delta\theta\}, \tag{29}$$

and

$$\widehat{\beta} = \{0, \Delta\beta, \cdots (T-1)\Delta\beta\}, \tag{30}$$

where $\Delta\theta = \frac{2\pi}{T}$ and $\Delta\beta = \frac{1}{T}$. The effective phase shifts and amplitude coefficients matrix $\widehat{\Phi}$ need to be selected from the above two sets in (29) and (30). Based on the proposed design at RISs, the interference residue at user k in cluster m can be transformed into

$$\widehat{I}_{m,k} = \left\| \mathbf{G}_{m,k}\widehat{\Phi}\mathbf{H}\sqrt{L_{m,k}}\mathbf{1}_M - \bar{\mathbf{W}}_{m,k}\sqrt{L_{b,m,k}}\mathbf{1}_{M-1} \right\|_2^2. \tag{31}$$

Hence, the SINR of user k in cluster m for the NI-RIS cases can be given by

$$\widehat{SINR}_{k,m} = \frac{\left|w^{m,k}\right|^2 L_{b,m,k}p\alpha_k^2}{\widehat{I}_{m,k}p + \sum\limits_{n=k+1}^{K} \left|w^{m,k}\right|^2 L_{b,m,k}p\alpha_n^2 + L\sigma^2}. \tag{32}$$

III. PERFORMANCE EVALUATION

In this section, new channel statistics, OPs, ERs, SE and EE are illustrated in the I-RIS cases.

A. New Channel Statistics

In this subsection, new channel statistics are derived for the proposed RIS-aided SCB design in a MIMO-NOMA network, which will be used for evaluating the network's performance.

Lemma 4. *Assuming that the fading channels of the BS-user links follow Rayleigh distribution. The elements of channel gains are independently and identically distributed (i.i.d.). The distribution of the effective channel gain of user k in cluster m for the I-RIS cases can be given by*

$$\left|w^{m,k}\right|^2 \sim \Gamma(L, 1), \tag{33}$$

where $\Gamma(\cdot, \cdot)$ represents the Gamma distribution.

Proof: Please refer to Appendix A. ∎

Then the PDF of the effective channel gain can be expressed as

$$f_1(x) = \frac{L^L x^{L-1}}{\Gamma(L)} e^{-Lx}. \tag{34}$$

B. OP and ER

We first focus on analyzing the OP of both the diffuse scattering and anomalous scattering scenarios. In this article, user k needs to decode the signals of the farer users by SIC technique, i.e. 1 to $k-1$ users, and hence the OP of user k in cluster m is defined by

$$P_{m,k} = 1 - \prod_{v=1}^{k-1} \mathbb{P}\left(\log_2(1 + SINR_{k\to v}) > R_v\right), \tag{35}$$

where R_v denotes the target rate of user v in cluster m, and $SINR_{k\to v} = \frac{|w^{m,k}|^2 L_{b,m,k} p\alpha_v^2}{\sum_{q=v+1}^{K} |w^{m,k}|^2 L_{b,m,k} p\alpha_q^2 + L\sigma^2}$.

Then the OP of user k in cluster m is given in the following Theorem.

Theorem 1. Let us assume that $\alpha_v^2 - \left(\sum_{q=v+1}^{K} \alpha_q^2\right)\varepsilon_v > 0$ with $v = 1, \cdots, k$, and the number of RISs obeys the constraints in **Lemma 1** as well as **Lemma 2**, the closed-form OP expression of user k in cluster m for the I-RIS cases can be expressed as

$$P_{m,k} = \frac{\gamma\left(L, I_{m,k*}\right)}{\Gamma(L)}, \tag{36}$$

where $I_{m,k*} = \max\{I_{m,1}, \cdots I_{m,k}\}$, $I_{m,v} = \frac{L\varepsilon_v \sigma^2 L_{b,m,k}}{p\left(\alpha_v^2 - \left(\sum_{q=v+1}^{K} \alpha_q^2\right)\varepsilon_v\right)}$, $\varepsilon_v = 2^{R_v} - 1$, and $\gamma(,)$ represents the lower incomplete Gamma function.

Proof: Recall that user k needs to decode the signal from user 1 to user $k-1$ one by one, and based on the OP defined in (35), the coverage probability can be written as

$$P_{m,k,\mathrm{C}} = 1 - \mathbb{P}\left(|w^{m,k}|^2 > I_{m,1}, \cdots, |w^{m,k}|^2 > I_{m,k}\right). \tag{37}$$

By applying $I_{m,k*} = \max\{I_{m,1}, \cdots I_{m,k}\}$, the coverage probability can be further transformed into

$$P_{m,k,\mathrm{C}} = 1 - \frac{\gamma\left(L, I_{m,k*}\right)}{\Gamma(L)}. \tag{38}$$

Hence, the results in (36) can be obtained. ∎

We then focus on the diversity orders of user k in cluster m, which can be obtained for evaluating the slope of OP.

Proposition 1. From **Theorem 1**, the diversity orders for the I-RIS cases can be determined by

expanding the lower incomplete Gamma function, and the diversity order of user k in cluster m of the proposed RIS-aided SCB design can be given by

$$d_{m,k} = -\lim_{\frac{p}{\sigma^2} \to \infty} \frac{\log P_{m,k}}{\log \frac{p}{\sigma^2}} \approx L, \tag{39}$$

Proof: Please refer to Appendix B. ∎

Remark 5. *Based on results in* (39)*, it is indicated that the diversity orders of all the NOMA users can be approximated to the number of RAs L for the I-RIS cases when the number of RISs is high enough.*

We then turn our attention to the ER of user K in cluster m, which is a salient metric for performance analysis, and hence the approximated ER expressions for user K in cluster m is given in the following Theorem.

Theorem 2. When the number of RISs N is sufficiently high, and $\alpha_v^2 - \left(\sum\limits_{q=v+1}^{K} \alpha_q^2 \right) \varepsilon_v > 0$ with $v = 1, \cdots, k$, the ER of user K in cluster m can be expressed in the closed-form as follows:

$$R_{m,K} = \frac{1}{\ln(2)} \sum_{i=0}^{L-1} \frac{C^i}{i!} \left(\exp(C) Ei(-C) + \sum_{a=1}^{i} (-1)^{a-1}(a-1)! C^a \right), \tag{40}$$

where $C = \frac{L\sigma^2}{p\alpha_K^2}$.

Proof: Please refer to Appendix C. ∎

Furthermore, the SINR of user k in cluster m may approach $SINR_{m,k} = \frac{\alpha_k^2}{\sum\limits_{q=k+1}^{K} \alpha_q^2}$ in the high-SNR regimes [40] based on the SINR analysis in (28). Hence, the expected rate of user k for $k = 1, \cdots, K-1$ can be written as $R_{m,k} = \log_2 \left(1 + \frac{\alpha_k^2}{\sum\limits_{q=k+1}^{K} \alpha_q^2} \right)$, which is a constant.

The high-SNR slope is defined as the asymptotic slope of the logarithmic plot of ER against the transmit power in dBm, which is a key parameter determining the ER in the high-SNR regimes, and hence the high-SNR slope can be expressed as

$$\Delta_{m,k} = -\lim_{\Xi \to \infty} \frac{R_{m,k}}{\log_2(1+\Xi)}, \tag{41}$$

where $\Xi = \frac{p}{\sigma^2}$.

Proposition 2. By substituting (40) into (41), the high-SNR slope of the nearest user can be given by

$$\Delta_{m,k} = 1. \tag{42}$$

Remark 6. *Based on the results in* (42)*, one can know that the high-SNR slopes of user K in each cluster of the I-RIS cases are one, which is not a function of the number of RISs.*

Remark 7. *Based on the SINR analysis in* (32) *and insights from [40], the high-SNR slopes of the $1, \cdots, K-1$-th NOMA users are 0 in both the I-RIS and NI-RIS cases.*

Remark 8. *Based on the SINR analysis in* (32)*, the diversity orders and high-SNR slopes of all the NOMA users are 0 in the NI-RIS cases.*

We then compare the OP of the proposed SCB enhanced MIMO-NOMA network and its OMA counterparts in the following Corollary, i.e. TDMA. The OMA counterparts adopted in this article is that by dividing the K users in equal time slots.

Corollary 1. *Let us assume that multiple users are divided in equal time slots in the OMA counterparts, the closed-form OP expression of user k in cluster m of the I-RIS cases is given by:*

$$\bar{P}_{m,k} = \frac{\gamma \left(L, I_{m,k,O} \right)}{\Gamma(L)}, , \tag{43}$$

where $I_{m,k,O} = \frac{L\varepsilon_O \sigma^2 L_{b,m,k}}{p}$, and $\varepsilon_O = 2^{KR_v} - 1$.

Proof: We first express the OP of user k in cluster m in the OMA counterparts as follows

$$\mathbb{P} \left\{ \frac{1}{K} log_2 \left(1 + SNR_{m,k,O} \right) > R_{m,k} \right\}, \tag{44}$$

where $SNR_{m,k,O} = \frac{pL_{b,m,k} \left| w^{m,k} \right|^2}{L\sigma^2}$. *Similar to Theorem 1, the results in* (43) *can be obtained.* ∎

C. SE and EE

Here, we focus on the SE of cluster m, which can be formulated based on the ER analysis in the previous subsection.

Proposition 3. In the proposed SCB design, the SE of cluster m can be given by

$$S_m = \sum_{k=1}^{K} R_{m,k}. \tag{45}$$

Since RISs are passive equipment, where only RIS controller needs power supply [41]–[43], hence we model the total dissipation power of the proposed SCB design as

$$P_e = P_{\text{B,s}} + KP_{\text{U}} + p\varepsilon_b + NP_L, \tag{46}$$

where $P_{\text{B,s}}$ and ε_b denote the power consumption and the efficiency of power amplifier at the BS, respectively. P_{U} and P_L denote the power consumption of each user and each RIS controller, respectively. Hence, the EE of the proposed design is given by the following Proposition.

Proposition 4. The EE of cluster m in the proposed SCB design can be given by

$$\Theta_{EE} = \frac{S_m}{P_e}, \tag{47}$$

where S_m and P_e are obtained from (45) *and* (46)*, respectively.*

IV. NUMERICAL RESULTS

In this section, numerical results are provided for the performance evaluation of the proposed SCB design. Monte Carlo simulations are provided for verifying the accuracy of our analytical results. The transmission bandwidth of the proposed network is set to $BW = 100$ MHz. In practice, the power of the AWGN is related to the bandwidth, which can be modeled as $\sigma^2 = -174 + 10\log_{10}(BW)$ dBm. For simplicity, the number of TAs is set to $M = 2$, and the number of users is set to $K = 2$. Based on NOMA protocol, the paired users share the power with the power allocation factors $\alpha_1^2 = 0.6$ and $\alpha_2^2 = 0.4$. The fading factors are set to $\mathcal{K}_1 = \mathcal{K}_{2,1} = \mathcal{K}_{2,2} = 3$. The distance of the BS-RIS links is set to $d_1 = 80$m, and the distance of the RIS-user links are set to $d_{1,2} = 80$m and $d_{1,1} = 160$m and those of the BS-user links are set to $d_{b,1,2} = 100$m and $d_{b,1,1} = 200$m. The path loss exponents of the BS-user links are set to $\alpha_3 = 3.5$ while those of the BS-RIS and RIS-user links are set to $\alpha_1 = \alpha_2 = 2.2$. The target rates are $R_2 = 1.5$ and $R_1 = 1$ bits per channel use (BPCU), unless otherwise clarified.

1) Minimal Required Number of RISs: In Fig. 2, we evaluate the minimal required number of RISs for implementing the proposed SCB design. On the one hand, observe that in the
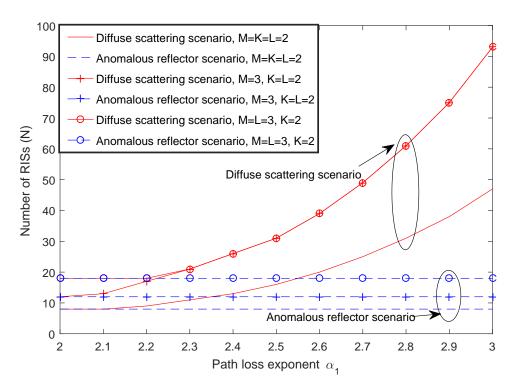
Fig. 2: Minimal required number of RISs for the I-RIS cases versus the path loss exponent.

anomalous reflector scenario, the minimal required number of RISs is only impacted by the number of TAs, RAs as well as the number of users. On the other hand, we can see that as the path loss exponent increases, the minimal required number of RISs increases for the diffuse scattering scenarios. This phenomenon indicates that the LoS links of both the BS-RIS and RIS-user links are required for implementing the proposed SCB design in the diffuse scattering scenarios, whereas the LoS links are not necessary for the anomalous reflector scenarios. Observe that for the case of $M = 3, K = L = 2$ as well as $M = L = 3, K = 2$, the minimal required RISs are identity, which indicates that the diffuse scattering scenario is more susceptible to the path loss exponent of both the BS-RIS and RIS-user links.

2) Impact of the Number of RAs: In Fig. 3, we evaluate the OP of the proposed SCB design in the RIS-aided MIMO-NOMA networks. We can see that as the number of RAs equipped at each user increases, the OP decreases. There are two reasons, where 1) since the precoding matrix is an identity matrix, and the detection vector is an all one vector, the RISs are capable of beneficially eliminating the inter-cluster interference in the I-RIS cases; 2) the received signal power can be significantly increased as more RAs are employed. One can observe that the slopes
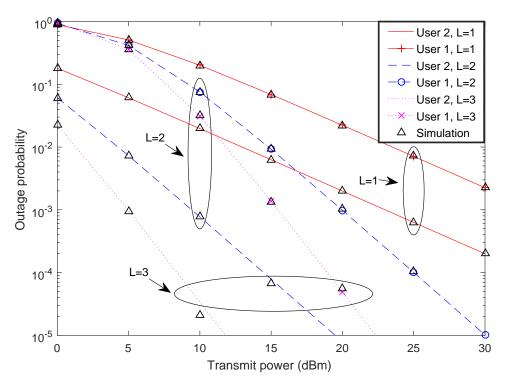
Fig. 3: OP of the I-RIS cases versus the transmit power with different number of RAs. The analytical results are calculated from (36). The number of RISs is set to $N = 5N_D$.

of the curves are approximated to the number of RAs, which validates our **Remark 5**.

3) Impact of the Number of Bits: In Fig. 4, we evaluate the OP of the paired NOMA users in the different number of bits, where the OP of the paired NOMA users in the I-RIS cases is provided as the benchmark schemes. We can see that as the transmit power increases, the OP floors occur. Observe that as the number of bits increases from 3-bit to 6-bit, the OP can be beneficially decreased. This is due to the fact that the higher number of bits is capable of increasing the resolution of each RIS element. It is also worth noting that 6-bit resolution is enough for obtaining the near-minimal OP, which indicates that the minimized OP is obtainable by appropriate setting the number of bits. Based on the simulation results, the diversity orders of the NI-RIS cases are zero, which verifies the insights gleaned from **Remark 8**.

4) Comparing ZF-based and SA-based Designs: In Fig. 5, combined with the insights inferred from [9], [10], we compare the OP of the paired NOMA users in the proposed RIS-aided SCB design, ZF-based design as well as SA-based design. In order to provide further engineering insights, we consider that the phase shifts and amplitude coefficients of RISs can be perfectly
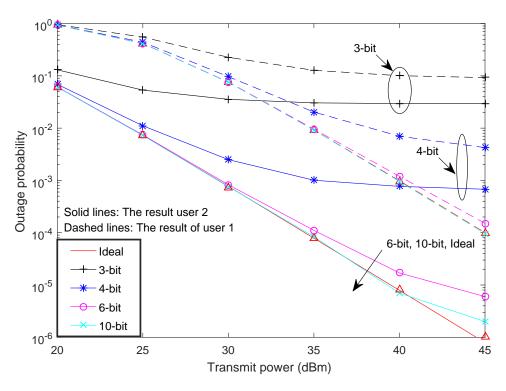
Fig. 4: OP of the NI-RIS cases versus the transmit power with different number of bits. The number of RISs is set to $N = 5N_D$.

TABLE III:
COMPARISON BETWEEN RIS-AIDED SCB, ZF-BASED AND SA-BASED DESIGNS. "MRN" DENOTES "MINIMAL REQUIRED NUMBER".

Mode	TAs	MRN of RAs	Antenna Gain
ZF-based [9]	M	$L \geq M$	$L - M + 1$
SA-based [10]	M	$L \geq \frac{M}{2} + 1$	L
RIS-aided SCB design	M	$L \geq 1$	L

manipulated. On the one hand, one can observe that the proposed RIS-aided design is capable of outperforming both the classic ZF-based and SA-based designs. On the other hand, the diversity order of the proposed RIS-aided design is L, which is higher than both the classic ZF-based and SA-based designs, and hence illustrate the benefits of the proposed RIS-aided SCB design. The detail of diversity orders is concluded in TABLE III.

5) Comparing RIS-aided NOMA and OMA networks: In Fig. 6, we evaluate the OP of both the RIS-aided NOMA and OMA networks. The OPs of NOMA and OMA networks are derived by $P_{\text{NOMA}} = P_{m,1} \times P_{m,2}$ and $P_{\text{OMA}} = \bar{P}_{m,1} \times \bar{P}_{m,2}$, respectively. As can be seen from Fig. 6, the
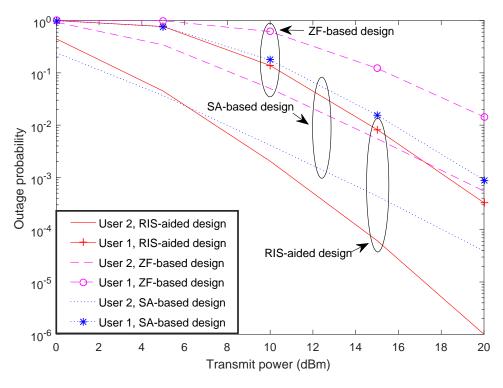
Fig. 5: OP of both the RIS-aided, ZF-based as well as SA-based designs versus the transmit power. The number of RAs is set to $L = 3$. The lengths of the RIS-user links are set to $d_{1,2} = 130$m and $d_{1,1} = 260$m and those of the BS-user links are set to $d_{b,1,2} = 150$m and $d_{b,1,1} = 240$m. The number of RISs is set to $N = 5N_D$.

OP of the RIS-aided NOMA networks is lower than that of the RIS-aided OMA networks, which implies that RIS-aided NOMA network is capable of providing better network performance than its OMA counterpart. Observed that for both the 3-bit and 4-bit resolutions, an optimal point exists due to the fact that there is a cross point of curves in the proposed SCB design. This indicates that the RIS-aided hybrid NOMA/OMA networks may be a good solution.

6) Impact of the Number of Bits on ER: We then evaluate the ER of the paired NOMA users versus the transmit power with the different number of bits in Fig. 7. Observe that as the transmit power increases, the ER ceilings occur in the NI-RIS cases. One can also observe that as the number of bits increases, the ER gaps between the I-RIS and NI-RIS cases are getting smaller. One can also observe that for the case of $b = 5$, the ER of both the NI-RIS and I-RIS cases are nearly identical, which indicates that the 5-bit finite resolution is high enough for the proposed RIS-aided SCB design. It is also worth noting that the ER of user 1 in cluster m is constant with the different number of bits, which also verifies the insights gleaned from **Remark 7**. Observed
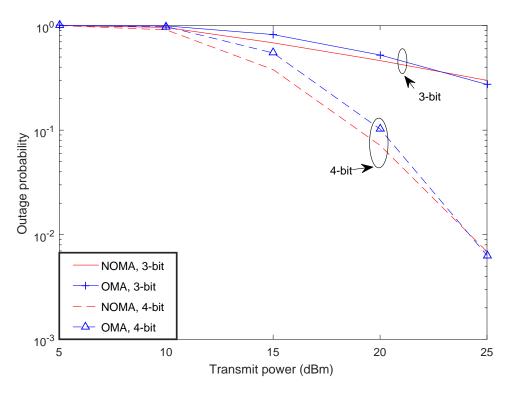
Fig. 6: OP of the NI-RIS cases in both the NOMA and OMA networks with different number of bits. The number of RISs is set to $N = 8N_D$.

that for the 3-bit and 4-bit resolutions, there exists an optimal number of RISs for maximizing the SE. This phenomenon also indicates that the RISs can be activated appropriately for enhancing the network's SE in the NI-RIS cases.

7) Spectrum Efficiency: In Fig. 8, we evaluate the SE of cluster m of the proposed RIS-aided SCB design. On the one hand, observe that the SE improves as the transmit power increases. However, as the increase of the number of RISs, observe that the slope of the SE is negative of the 3-bit cases, which indicates that there exists an optimal value of the number of RISs that maximizes the SE. It is also worth noting that the SE of the 4-bit cases are nearly identical compared to the 3-bit cases, which indicates that the RIS-aided SCB design with 4-bit finite resolutions becomes more competitive.

8) Energy Efficiency: We then evaluate the EE of the proposed SCB design in Fig. 9. Several observations can be concluded as: 1) One can observe that the slopes of EE are negative in the NI-RIS cases. This is due to the fact that in the proposed SCB design, the main goal of passive beamforming is to eliminate the inter-cluster interference, and hence the maximum EE is fixed,
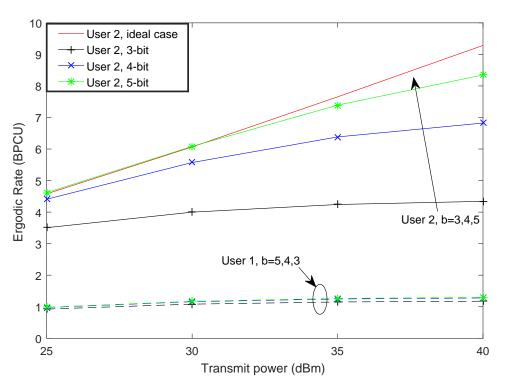
Fig. 7: ER of the NI-RIS cases versus the number of RISs with different number of bits. The number of RISs is set to $N = 5N_D$.

which leads to the low EE when the number of RISs is too high; 2) The EE increases as the number of bits increase, this is due to the fact that the inter-cluster interference residue decreases when there are more potential solutions at RISs; and 3) Based on the fact that the EE curve decreases, it is readily to observe that there exists an optimal value of the number of RISs.

V. Conclusions

We first reviewed previous contributions related to the RIS-aided SEB designs in this article, and we then proposed a novel RIS-aided SCB design. In order to provide a general design of RIS networks, we adopted a MIMO-NOMA network, where the passive beamforming weights of the RISs were designed. The channel statistics, OPs, ERs, SE as well as EE were derived in closed-form for characterizing the system performance. Compared to the previous ZF-based and SA-based designs, the proposed RIS-aided SCB design releases the constraint of the number of RAs. An important future direction is to minimize the required number of RISs and RAs by jointly designing both the active beamforming, passive beamforming, and detection vectors.
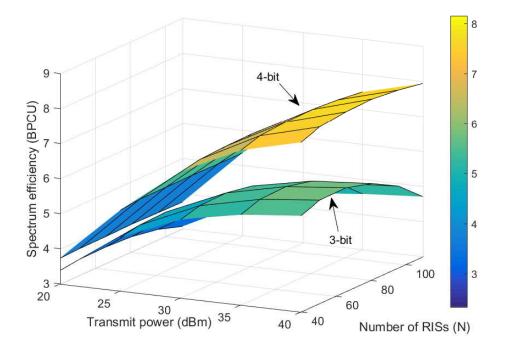
Fig. 8: SE of the NI-RIS cases versus the number of RISs with different number of bits.

APPENDIX A: PROOF OF LEMMA 4

Recall that the effective channel vector $\mathbf{w}_m^{m,k}$ contains L elements, and by utilizing the proposed detection vector at the users, we can obtain the following channel gain:

$$\left|w^{m,k}\right|^2 = \sum_{l=1}^{L} \left|w_{l,1}^{m,k}\right|^2. \tag{A.1}$$

Based on the result derived in (A.1), and exploiting the fact that the elements of $|\mathbf{W}_{m,k}|$ are i.i.d., the mean and variance of the effective channel gain can be given by using the property of random variables as follows

$$E_1 = \sum_{l=1}^{L} \mathbb{E}\left(\left|w_{l,1}^{m,k}\right|^2\right) = L, \tag{A.2}$$

and

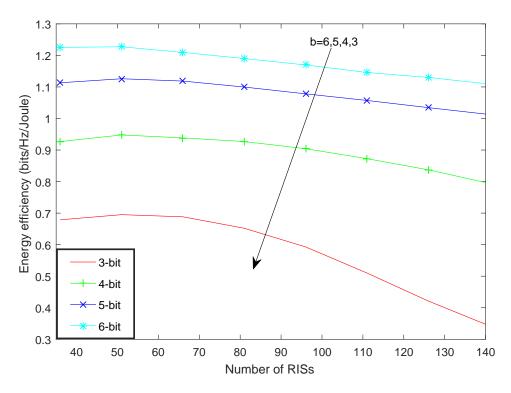$$V_1 = \sum_{l=1}^{L} \mathbb{V}\left(\left|w_{l,1}^{m,k}\right|^2\right) = L. \tag{A.3}$$

Fig. 9: EE of the NI-RIS cases versus the number of RISs with different number of bits.

Thus, the effective channel gain can be rewritten as

$$\left| w^{m,k} \right|^2 \sim (L, L). \tag{A.4}$$

Hence, the effective channel gain can be obtained in a more elegant form in (33).

APPENDIX B: PROOF OF PROPOSITION 1

In order to glean the diversity order of the proposed SCB design, the lower incomplete Gamma function can be expanded as follows [44]:

$$\gamma (L, I_{m,k*}) = \sum_{s=0}^{\infty} \frac{\Gamma (L)}{\Gamma (L + s + 1)} (I_{m,k*})^{L+s} \exp (-I_{m,k*}). \tag{B.1}$$

When replacing $\exp(-I_{m,k*})$ by its power series expansion, the OP can be further transformed into

$$\bar{P}_{m,k} = (I_{m,k*})^L \sum_{s=0}^{\infty} \frac{(-I_{m,k*})^s}{s! (L + s)}. \tag{B.2}$$

Thus, by applying the definition of diversity order, the results in (39) can be gleaned, and the

proof is complete.

APPENDIX C: PROOF OF THEOREM 2

The proof starts by expressing the ER of user K in cluster m as follows:

$$R_{m,K} = \mathbb{E}\left\{\log_2\left(1 + SINR_{m,K}\left(x\right)\right)\right\}$$
$$= -\int_0^\infty \log_2(1+x)d\left(1 - F\left(x\right)\right) \tag{B.1}$$
$$= \frac{1}{\ln\left(2\right)}\int_0^\infty \frac{1 - F\left(x\right)}{1+x}dx.$$

The cumulative distribution function of user K in cluster m can be calculated as

$$F\left(x\right) = \left(\frac{\gamma\left(L, Cx\right)}{\Gamma(L)}\right). \tag{B.2}$$

Based on expression in (B.1), the lower incomplete Gamma function ought to be expanded with a constant for obtaining the closed-form expressions, hence we expand the lower incomplete Gamma function as follows:

$$\frac{\gamma\left(L, Cx\right)}{\Gamma(L)} = 1 - \sum_{i=0}^{L-1}\frac{\left(Cx\right)^i}{i!}e^{-Cx}. \tag{B.3}$$

Thus, the ER can be written as

$$R_{m,K} = \frac{1}{\ln\left(2\right)}\sum_{i=0}^{L-1}\frac{C^i}{i!}\int_0^\infty \frac{x^i e^{-Cx}}{1+x}dx. \tag{B.4}$$

Hence, the tractable approximated results can be derived as

$$R_{m,K} = \frac{1}{\ln\left(2\right)}\sum_{i=0}^{L-1}\frac{C^i}{i!}\left(\exp(C)Ei(-C) + \sum_{a=1}^{i}(-1)^{a-1}(a-1)!C^a\right). \tag{B.5}$$

Hence, the ER of user K in cluster M is obtained in (40), and the proof is complete.

REFERENCES

[1] T. Hou, Y. Liu, Z. Song, X. Sun, and Y. Chen, "A simple design for RIS-aided MIMO-NOMA networks," in *2020 IEEE GLOBECOM*, Dec. 2020, pp. 1–6.

[2] S. Lien, S. Shieh, Y. Huang, B. Su, Y. Hsu, and H. Wei, "5G new radio: Waveform, frame structure, multiple access, and initial access," *IEEE Commun. Mag.*, vol. 55, no. 6, pp. 64–71, Jun. 2017.

[3] Z. Ding, Y. Liu, J. Choi, Q. Sun, M. Elkashlan, C. I, and H. V. Poor, "Application of non-orthogonal multiple access in LTE and 5G networks," *IEEE Commun. Mag.*, vol. 55, no. 2, pp. 185–191, Feb. 2017.

[4] Z. Ding, P. Fan, and H. V. Poor, "Impact of user pairing on 5G nonorthogonal multiple-access downlink transmissions," *IEEE Trans. Veh. Technol.*, vol. 65, no. 8, pp. 6010–6023, Aug. 2016.

[5] M. Shirvanimoghaddam, M. Dohler, and S. J. Johnson, "Massive non-orthogonal multiple access for cellular IoT: Potentials and limitations," *IEEE Commun. Mag.*, vol. 55, no. 9, pp. 55–61, Sep. 2017.

[6] Y. Liu, Z. Qin, M. Elkashlan, Z. Ding, A. Nallanathan, and L. Hanzo, "Nonorthogonal multiple access for 5G and beyond," *Proc. of the IEEE*, vol. 105, no. 12, pp. 2347–2381, Dec. 2017.

[7] S. M. R. Islam, N. Avazov, O. A. Dobre, and K. Kwak, "Power-domain non-orthogonal multiple access (NOMA) in 5G systems: Potentials and challenges," *IEEE Commun. Surveys Tuts.*, vol. 19, no. 2, pp. 721–742, Secondquarter 2017.

[8] Y. Liu, Z. Qin, M. Elkashlan, A. Nallanathan, and J. A. McCann, "Non-orthogonal multiple access in large-scale heterogeneous networks," *IEEE J. Sel. Areas Commun.*, vol. 35, no. 12, pp. 2667–2680, Dec. 2017.

[9] Z. Ding, F. Adachi, and H. V. Poor, "The application of MIMO to non-orthogonal multiple access," *IEEE Trans. Wireless Commun.*, vol. 15, no. 1, pp. 537–552, Jan. 2016.

[10] Z. Ding, R. Schober, and H. V. Poor, "A general MIMO framework for NOMA downlink and uplink transmission based on signal alignment," *IEEE Trans. Wireless Commun.*, vol. 15, no. 6, pp. 4438–4454, Jun. 2016.

[11] M. Zeng, A. Yadav, O. A. Dobre, G. I. Tsiropoulos, and H. V. Poor, "Capacity comparison between MIMO-NOMA and MIMO-OMA with multiple users in a cluster," *IEEE J. Sel. Areas Commun.*, vol. 35, no. 10, pp. 2413–2424, Oct. 2017.

[12] Y. Liu, Z. Qin, M. Elkashlan, Y. Gao, and L. Hanzo, "Enhancing the physical layer security of non-orthogonal multiple access in large-scale networks," *IEEE Trans. Wireless Commun.*, vol. 16, no. 3, pp. 1656–1672, Mar. 2017.

[13] Y. Liu, Z. Ding, M. Elkashlan, and H. V. Poor, "Cooperative non-orthogonal multiple access with simultaneous wireless information and power transfer," *IEEE J. Sel. Areas Commun.*, vol. 34, no. 4, pp. 938–953, Apr. 2016.

[14] J. Zhang, E. Bjrnson, M. Matthaiou, D. W. K. Ng, H. Yang, and D. J. Love, "Multiple antenna technologies for beyond 5G," *Arxiv*, vol. 1910.00092, Sep. 2019.

[15] Y. Liang, R. Long, Q. Zhang, J. Chen, H. V. Cheng, and H. Guo, "Large intelligent surface/antennas (LISA): Making reflective radios smart," *J. Commun. Inf. Networks*, vol. 4, no. 2, pp. 40–50, Jun. 2019.

[16] E. Basar, "Transmission through large intelligent surfaces: A new frontier in wireless communications," *Arxiv*, vol. 1902.08463v2, Apr. 2019.

[17] S. Parkvall, E. Dahlman, A. Furuskar, and M. Frenne, "NR: The new 5G radio access technology," *IEEE Commun. Standards Mag.*, vol. 1, no. 4, pp. 24–30, Dec. 2017.

[18] Q. Wu and R. Zhang, "Towards smart and reconfigurable environment: Intelligent reflecting surface aided wireless network," *Arxiv*, vol. 1905.00152v3, Jun. 2019.

[19] M. D. Renzo *et al.*, "Smart radio environments empowered by AI reconfigurable meta-surfaces: An idea whose time has come," *Arxiv*, vol. 1903.08925, Mar. 2019.

[20] M. D. Renzo and J. Song, "Reflection probability in wireless networks with metasurface-coated environmental objects: An approach based on random spatial processes," *Arxiv*, vol. 1901.01046v1, Jan. 2019.

[21] T. Hou, Y. Liu, Z. Song, X. Sun, Y. Chen, and L. Hanzo, "MIMO assisted networks relying on large intelligent surfaces: A stochastic geometry model," *arXiv*, vol. 1910.00959v1, pp. 1–1, Oct. 2019.

[22] H. Lu, Y. Zeng, S. Jin, and R. Zhang, "Enabling panoramic full-angle reflection via aerial intelligent reflecting surface," in *Arxiv*, Jan. 2020, pp. 1–6.

[23] M. D. Renzo, F. H. Danufane, X. Xi, J. de Rosny, and S. Tretyakov, "Analytical modeling of the path-loss for reconfigurable intelligent surfaces anomalous mirror or scatterer?" *Arxiv*, vol. 2001.10862v1, pp. 1–1, Jan. 2020.

[24] N. S. Perovi, M. D. Renzo, and M. F. Flanagan, "Channel capacity optimization using reconfigurable intelligent surfaces in indoor mmWave environments," *arXiv*, vol. 1910.14310v1, pp. 1–1, Oct. 2019.

[25] Y. Cao and T. Lv, "Intelligent reflecting surface aided multi-user millimeter-wave communications for coverage enhancement," *arXiv*, vol. 1910.02398v1, pp. 1–1, Oct. 2019.

[26] Z. Ding and H. V. Poor, "A simple design of IRS-NOMA transmission," *arXiv*, vol. 1907.09918v2, pp. 1–1, Jul. 2019.

[27] X. Yue and Y. Liu, "Performance analysis of intelligent reflecting surface assisted NOMA networks," *Arxiv*, vol. 2002.09907v1, pp. 1–1, Feb. 2020.

[28] X. Yu, D. Xu, and R. Schober, "MISO wireless communication systems via intelligent reflecting surfaces," *Arxiv*, vol. 1904.12199v1, Apr. 2019.

[29] G. Yang, X. Xu, and Y. Liang, "Intelligent reflecting surface assisted non-orthogonal multiple access," *Arxiv*, vol. 1907.03133v1, Jul. 2019.

[30] T. Hou, Y. Liu, Z. Song, X. Sun, Y. Chen, and L. Hanzo, "Reconfigurable intelligent surface aided NOMA networks," *arXiv*, vol. 1912.10044v1, pp. 1–1, Dec. 2019.

[31] H. Han, J. Zhao, D. Niyato, M. D. Renzo, and Q. Pham, "Intelligent reflecting surface aided network: Power control for physical-layer broadcasting," *arXiv*, vol. 1910.14383v1, pp. 1–1, Oct. 2019.

[32] X. Guan, Q. Wu, and R. Zhang, "Intelligent reflecting surface assisted secrecy communication via joint beamforming and jamming," *arXiv*, vol. 1907.12839v3, pp. 1–1, Jul. 2019.

[33] K. Ntontin, J. Song, and M. D. Renzo, "Multi-antenna relaying and reconfigurable intelligent surfaces: End-to-end SNR and achievable rate," *Arxiv*, vol. 1908.07967v2, pp. 1–1, Aug. 2019.

[34] F. P. Fontàn and P. M. Espiñeira, *Modelling the wireless propagation channel: A simulation approach with MATLAB*. John Wiley, 2008.

[35] R. G. Winter and A. M. Steinberg, *Coherence*. Access Science. McGraw-Hill., 2008.

[36] Q. Wu and R. Zhang, "Beamforming optimization for wireless network aided by intelligent reflecting surface with discrete phase shifts," *Arxiv*, vol. 1906.03165v2, Jun. 2019.

[37] S. Zhang and R. Zhang, "Capacity characterization for intelligent reflecting surface aided MIMO communication," *Arxiv*, vol. 1910.13636v1, Oct. 2019.

[38] B. Zheng, Q. Wu, and R. Zhang, "Intelligent reflecting surface-assisted multiple access with user pairing: NOMA or OMA?" *Arxiv*, vol. 2001.08909v2, pp. 1–1, Jan. 2020.

[39] X. Mu, Y. Liu, L. Guo, J. Lin, and N. Al-Dhahir, "Exploiting intelligent reflecting surfaces in multi-antenna aided NOMA systems," *Arxiv*, vol. 1910.13636v1, Oct. 2019.

[40] T. Hou, Y. Liu, Z. Song, X. Sun, and Y. Chen, "Multiple antenna aided NOMA in UAV networks: A stochastic geometry approach," *IEEE Trans. Commun.*, vol. 67, no. 2, pp. 1031–1044, Feb. 2019.

[41] L. N. Ribeiro, S. Schwarz, M. Rupp, and A. L. F. de Almeida, "Energy efficiency of mmWave massive MIMO precoding with low-resolution DACs," *IEEE J. Sel. Topics Signal Process*, vol. 12, no. 2, pp. 298–312, May 2018.

[42] C. Huang, G. C. Alexandropoulos, A. Zappone, M. Debbah, and C. Yuen, "Energy efficient multi-user MISO communication using low resolution large intelligent surfaces," in *2018 IEEE GLOBECOM Workshops (GC Wkshps)*, Dec. 2018, pp. 1–6.

[43] C. Huang, A. Zappone, G. Alexandropoulos, M. Debbah, and C. Yuen, "Reconfigurable intelligent surfaces for energy efficiency in wireless communication," *Arxiv*, vol. 1810.06934v5, Jun. 2019.

[44] I. S. Gradshteyn and I. M. Ryzhik, *Table of Integrals, Series and Products*. New York: Academic Press, 6th ed, 2000.